

TeCoNeRV: Leveraging Temporal Coherence for Compressible Neural Representations for Videos

Namitha Padmanabhan¹ Matthew Gwilliam¹ Abhinav Shrivastava¹

Abstract

Implicit Neural Representations (INRs) have recently demonstrated impressive performance for video compression. However, since a separate INR must be overfit for each video, scaling to high-resolution videos while maintaining encoding efficiency remains a significant challenge. Hypernetwork-based approaches predict INR weights (hyponetworks) for unseen videos at high speeds, but with low quality, large compressed size, and prohibitive memory needs at higher resolutions. We address these fundamental limitations through three key contributions: (1) an approach that decomposes the weight prediction task spatially and temporally, by breaking short video segments into patch tubelets, to reduce the pretraining memory overhead by $20\times$; (2) a residual-based storage scheme that captures only differences between consecutive segment representations, significantly reducing bitstream size; and (3) a temporal coherence regularization framework that encourages changes in the weight space to be correlated with video content. Our proposed method, TeCoNeRV, achieves substantial improvements of 2.47dB and 5.35dB PSNR over the baseline at 480p and 720p on UVG, with 36% lower bitrates and 1.5-3 \times faster encoding speeds. With our low memory usage, we are the first hypernetwork approach to demonstrate results at 480p, 720p and 1080p on UVG, HEVC and MCL-JCV. Our project page is available [here](#).

1. Introduction

Video data continues to dominate internet traffic, creating an ever-growing need for efficient compression. Conventional block-based video codecs (Le Gall, 1991; Wiegand et al., 2003; Sullivan et al., 2012b) establish strong compression-quality tradeoffs through decades of engineering, while neural compression methods (Rippel et al., 2019; Khani et al.,

¹Department of Computer Science, University of Maryland, College Park, USA. Correspondence to: Namitha Padmanabhan <namithap@umd.edu>.

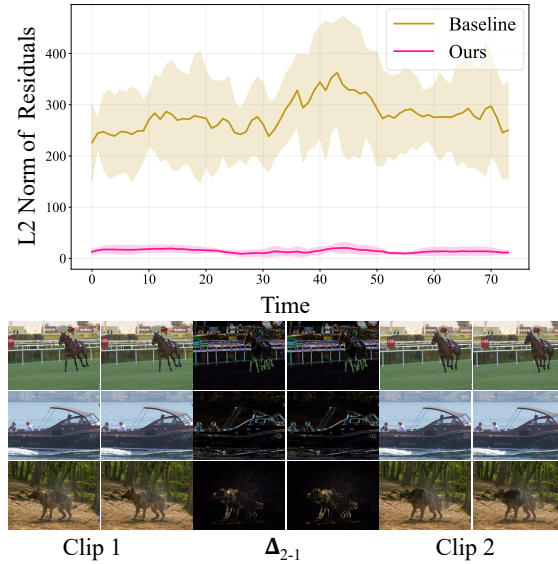


Figure 1. TeCoNeRV achieves smoother weight transitions across video clips, enabling superior compression. Bottom: Selected frames from consecutive clips of three videos from the UVG dataset, with the change in pixel space visualized in the middle column. Top: L2 norm of clip-to-clip weight residuals over time for the baseline (NeRV-Enc (Chen et al., 2024)) versus our approach (TeCoNeRV). Our temporal coherence regularization produces smaller weight residuals as video content evolves, resulting in efficient compression while preserving visual quality.

2021; Li et al., 2021; 2023) offer quality and size improvements, although at the cost of slower decoding. Recently, Implicit Neural Representations (INRs) have shown promise by representing videos as compact neural networks (Chen et al., 2021; Kwan et al., 2023; Kim et al., 2024), achieving fast decoding speeds through simple feed-forward operations. However, traditional INRs train a separate neural network for each video, making encoding prohibitively slow for practical applications. To address the problem of INR encoding efficiency, hypernetwork methods train a single network to predict the weights of the individual INRs (called “hyponetworks”) for unseen videos (Chen & Wang, 2022; Kim et al., 2022; Chen et al., 2024). However, prior hypernetwork compression works demonstrate results only at low resolutions (256×256), for sparse framerates (8 to 16 frames per video), and with large compressed sizes.

We propose TeCoNeRV, a framework for adapting INR hypernetworks to compress videos efficiently at higher resolutions. Using prior works, predicting hyponetwork weights becomes computationally prohibitive, since memory requirements scale quadratically as resolution increases. We address this fundamental scaling limitation by introducing a patch-tubelet approach that decomposes each clip into smaller spatio-temporal volumes. This decomposition (i) alleviates the memory requirements for predicting large hyponetworks, and (ii) directly lends itself to inference at higher frame resolutions. The latter is possible even when the patch size is not a perfect factor of the frame size because we can employ strided patches with overlap. We simply crop at the patch boundaries to ensure smooth transitions. This unlocks a huge benefit: resolution-independent training. For example, we can train our model on 480p videos and perform inference at 1080p.

Further, we analyze the implicit weight representations produced by existing hypernetwork systems for videos. We find that naïve hypernetwork predictions generate weights that can vary dramatically for adjacent frames (Figure 1, top panel), even when visual changes are minor (bottom panel). We argue that smooth pixel transitions should correspond to smooth weight transitions for better compression. Therefore, we introduce a temporal coherence regularization that conditions weight spaces to evolve smoothly with changes in adjacent clips. Applied as finetuning after initial training, this naturally induces sparsity in weight transitions. This regularization dramatically reduces both the magnitude and variance of weight residuals across clips, as evidenced by the lower and more consistent L2 norm curve of our approach in Figure 1, compared to the baseline (NeRV-Enc (Chen et al., 2024)). We store only the first clip’s full weights and compact residuals for subsequent clips, significantly reducing bitstream size without sacrificing quality. The strength of the regularization can thus serve as a rate control mechanism.

At inference time, our method processes the target video clip-by-clip, predicting hyponetwork weights for each patch position and storing only the first prediction along with subsequent compact residuals. This approach maintains encoding speeds comparable to NeRV-Enc (Chen et al., 2024) while achieving superior compression and reconstruction quality. This architecture achieves substantial improvements over the baseline on the UVG dataset (Mercat et al., 2020): 2.47dB PSNR gain at 480p and 5.35dB gain at 720p, with a 36% reduction in bitrate, while maintaining practical encoding speeds. We also show consistent gains on the diverse Kinetics-400 (Kay et al., 2017), HEVC (Ohm et al., 2012) and MCL-JCV (Wang et al., 2016a) datasets. In addition, encoding residuals over individual clip weights significantly improves encoding speed. We summarize our main contributions below:

- TeCoNeRV, the first hypernetwork-based approach that successfully scales to higher resolution video compression by addressing fundamental limitations in memory usage and encoding efficiency. We achieve this through a patch-tubelet decomposition strategy that divides the weight prediction task spatially and temporally.
- A residual encoding strategy that dramatically reduces bitstream size by exploiting temporal redundancy between consecutive clips.
- Rate control with weight-space conditioning that aligns hyponetwork evolution with video content, ensuring smoother transitions that produce smaller, more consistent residuals across clips for further compression.
- Resolution-independent training – we can predict high resolution videos using models trained at any resolution.

2. Related Work

Video Compression. Traditional video codecs (Le Gall, 1991; Wiegand et al., 2003; Sullivan et al., 2012b) employ block-based motion estimation and compensation techniques to achieve acceptable compression-quality tradeoffs. With the rise of deep learning, many works have sought to improve or replace components of these pipelines (Li et al., 2021; Rippel et al., 2019; Khani et al., 2021; Li et al., 2023; 2024). The NVC and DCVC family (Li et al., 2021; 2023; 2024) achieves competitive rate-distortion performance through techniques like contextual entropy modeling and temporal feature modulation. Through years of operational cost optimization, DCVC-RT (Jia et al., 2025) achieves real-time performance for 1080p encoding. While these methods excel in compression ratio, INR-based approaches offer complementary advantages including fast decoding without complex motion modules, compact storage, and support for continuous spatiotemporal interpolation.

Implicit Neural Representations. INRs encode signals such as images, videos, or 3D scenes as neural networks that map continuous coordinates to signal values (Mildenhall et al., 2020; Sitzmann et al., 2020a). For images, they map spatial coordinates (x, y) to RGB values (Tancik et al., 2020; Dupont et al., 2021; 2022; Ladune et al., 2023), while for videos, they incorporate temporal coordinates (t) (Zhang et al., 2021; Kim et al., 2024), offering compact storage suitable for compression tasks. NeRV (Chen et al., 2021) maps time embeddings to entire frames, spawning a family of video INRs (Chen et al., 2023; Kwan et al., 2023; Lee et al., 2023; He et al., 2023; Li et al., 2022; Yan et al., 2024; Zhao et al., 2023) advancing different aspects of frame-wise representation. Recent works model flow in standard INRs (Lee et al., 2023; Shin et al., 2024) or optimize spatio-temporal patches directly for static signals (Saragadam et al., 2022;

Ashkenazi & Treister, 2024). In contrast, our method operates in the generalizable hypernetwork paradigm for videos, without explicit flow modeling, and leverages temporal coherence to encourage small residuals between similar frame groups. NIRVANA (Maiya et al., 2023) addresses encoding efficiency by encoding frame group patches autoregressively, however it still requires per-video optimization, taking hours to encode. Our hypernetwork approach eliminates per-video optimization entirely.

Hypernetworks. To address the per-sample long encoding times that INR suffer from, several works have explored hypernetworks – neural networks that predict the weights of another network (the hyponetwork). Some works demonstrate hypernetwork approaches for 3D scenes (Sitzmann et al., 2020b; Chiang et al., 2022; Sen et al., 2022; 2023) while others focus on predicting INRs to generate images (Skorokhodov et al., 2021) or videos (Yu et al., 2022). Recent work focuses on hypernetworks predicting INR weights to reconstruct inputs (Chen & Wang, 2022; Kim et al., 2022; Maiya et al., 2024). FastNeRV (Chen et al., 2021) introduces a single hypernetwork for frame-wise video representation with faster encoding speeds than pixel-wise approaches. However, existing hypernetwork compression methods struggle with low quality and practical resolutions and video lengths. We address these scalability challenges through patch-tubelet decomposition, combined with residual encoding and temporal coherence regularization to improve compression efficiency.

Feature Representation Learning. Our temporal coherence approach draws inspiration from self-supervised learning techniques (Chen et al., 2020; He et al., 2020; Grill et al., 2020; Sun et al., 2021) that exploit temporal structure in videos. Jayaraman & Grauman (2016) employ unsupervised contrastive loss to learn representations that change smoothly with visual transformations, extending earlier slow feature analysis work (Wiskott & Sejnowski, 2002; Hurri & Hyvärinen, 2003). Other methods use time as a semantic similarity proxy (Sermanet et al., 2018), predict future latents (Oord et al., 2018), or exploit temporal order as supervision (Wang et al., 2016b; Lee et al., 2017; Misra et al., 2016). These insights motivate our approach – conditioning weights to evolve synchronously with temporal progression exploits video continuity for compression efficiency.

3. Method

3.1. Background and Problem Formulation

Given an input video $V \in \mathbb{R}^{T \times 3 \times H \times W}$ with T frames at spatial resolution $H \times W$, an INR represents the video as a neural network f_θ mapping spatial and temporal coordinates to RGB pixel values. We build upon NeRV-Enc/NeRV-Dec (Chen et al., 2024), which uses a hypernetwork g_ϕ to

predict weights of a NeRV (Chen et al., 2021) video representation (HypoNeRV). Unlike NeRV-Enc’s sparse frame sampling, we process consecutive frame sequences (clips): $S \in \mathbb{R}^{N \times 3 \times H \times W}$, where N is the clip length. For each clip, g_ϕ predicts weights of the hyponetwork f_θ to reconstruct all frames in the sequence. The hyponetwork follows the NeRV architecture with time positional encoding and NeRV blocks (convolution + PixelShuffle (Shi et al., 2016)). The learnable parameters comprise: (1) video-agnostic base parameters θ_{base} , shared across all videos, and (2) clip-specific unique parameters θ_{uniq} , generated by the hypernetwork encoder from input data tokens and learnable weight tokens. The final hyponetwork weights θ are obtained by modulating the base parameters with expanded unique parameters, through element-wise multiplication. This system is optimized via mean squared error between reconstructed and ground truth frames:

$$(\phi^*, \theta_{\text{base}}^*) = \underset{\phi, \theta_{\text{base}}, \theta_{\text{uniq}}}{\operatorname{argmin}} \sum_{V \in D_{\text{train}}} \sum_S \sum_t \|f_{\theta=g_\phi(S)}(t) - \mathbf{S}_t\|_2^2 \quad (1)$$

where D_{train} is the training dataset, S are clips from video V , and t indexes frames within each clip.

In the following sections, we explain the main components of our proposed method – a novel training paradigm for high-resolution videos, differential encoding of clip weights using residuals and finally, the weight space regularization framework for temporal coherence.

3.2. Scaling to Higher Resolution Videos

A key challenge with prior hypernetwork-based approaches is that memory requirements scale quadratically with video resolution, making direct application to higher-resolution videos (720p+) infeasible. To address this limitation, we introduce patch-tubelets (Figure 2), which enable our approach to scale efficiently to higher resolutions. We partition each clip $S \in \mathbb{R}^{N \times 3 \times H \times W}$ into patch tubelets $P \in \mathbb{R}^{N \times 3 \times H_p \times W_p}$, where $H_p \ll H$ and $W_p \ll W$ represent the spatial dimensions of each patch. This decomposition reduces the problem from predicting weights for entire frames to localized spatio-temporal volumes, making the weight prediction problem more tractable. This approach offers two advantages: memory efficiency, as requirements depend on patch dimensions rather than full-frame dimensions; and resolution independence, as the hypernetwork processes fixed-size patches regardless of the full video resolution. At inference time, we predict hyponetwork weights for each spatial position and combine their outputs to reconstruct full-resolution frames. Quality metrics are computed at native resolution to ensure fidelity to the original signal. This methodology is inherently scalable to higher resolutions, as computationally complexity grows linearly with the number of patches rather than quadratically with resolution.

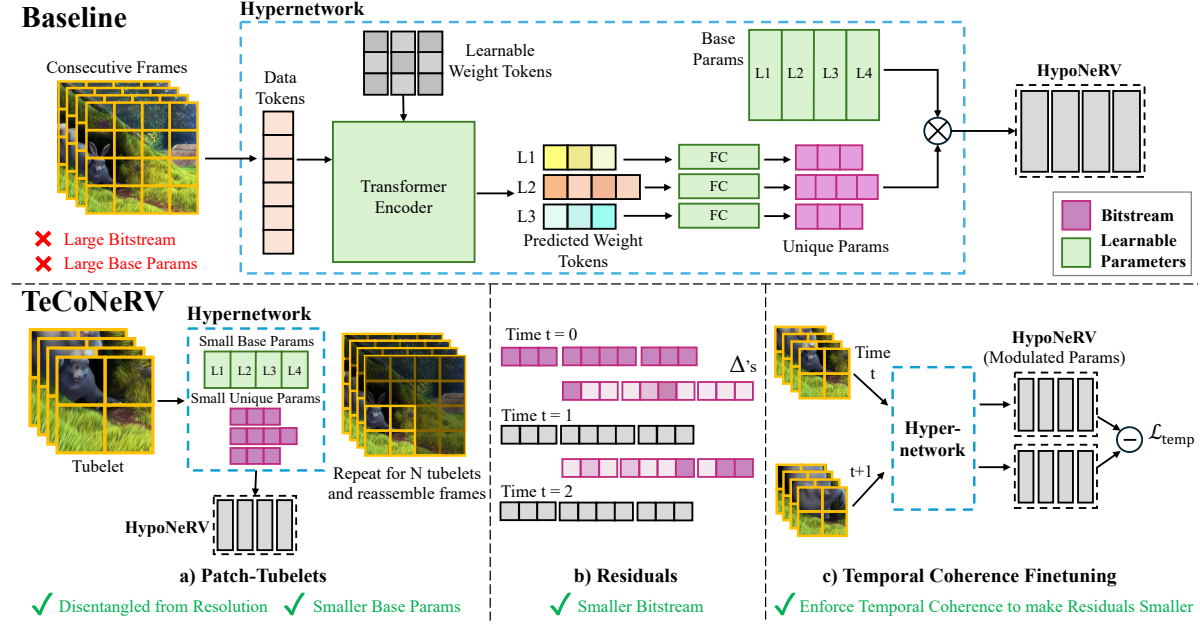


Figure 2. Overview of TeCoNeRV. Above: Hypernetworks from prior work predict weights for entire video frames at once, resulting in large base parameters and bitstream size. Below: Our approach with (a) patch-tubelets that decouple spatial resolution from memory requirements, (b) residual encoding that stores only weight differences across time steps, and (c) temporal coherence finetuning that regularizes weight differences. Together, these components achieve better compression efficiency and superior reconstruction quality.

3.3. Residuals: Compression and Storage

We improve compression efficiency by exploiting temporal redundancy across consecutive clips. Instead of storing complete unique parameters for each clip, we implement a differential encoding scheme where for each spatial position (patch tubelet) in the video, we store complete unique parameters θ_{unq} only for the first clip and compact residuals for subsequent clips. During decoding, clip parameters are reconstructed via cumulative addition before modulating with the shared base parameters installed as part of the decoder. This approach is particularly effective for consecutive frames with similar content, where weight transitions are small. The compression becomes even more effective when combined with our temporal coherence regularization described next. For the final compressed bitstream, we apply uniform quantization to the first hyponetwork weights and residuals followed by arithmetic coding (Witten et al., 1987), without requiring quantization-aware training.

3.4. Temporal Coherence Regularization

While residual encoding exploits redundancy, hypernetworks trained solely for reconstruction do not inherently produce weight spaces that transition smoothly over time. Thus, hyponetwork predictions can vary dramatically between clips with similar visual elements. This phenomenon is also observed in per-video INRs optimized with pixel-level losses; prior analysis reveals that individual neurons

do not maintain stable correspondence to semantic entities over time (Padmanabhan et al., 2024). Thus, even visually smooth transitions can induce abrupt changes in the weight space. To address this, we introduce a temporal coherence regularization that explicitly conditions hyponetwork weights to evolve with video content. This is applied as a finetuning step after training, with the combined objective:

$$(\phi^*, \theta_{\text{base}}^*) = \underset{\phi, \theta_{\text{base}}, \theta_{\text{unq}}}{\operatorname{argmin}} \mathcal{L}_{\text{recon}}(\phi, \theta) + \lambda_{\text{temp}} \mathcal{L}_{\text{temp}}(\theta) \quad (2)$$

where $\mathcal{L}_{\text{recon}}(\phi, \theta)$ is the MSE loss from Equation (1), $\mathcal{L}_{\text{temp}}$ is our unsupervised temporal regularization loss, and λ_{temp} is the hyperparameter that controls the regularization strength. To implement this loss, we construct a dataset of consecutive patch-tubelet pairs, D_{reg} (Jayaraman & Grauman, 2016):

$$D_{\text{reg}} = \{(i, i+1) : P_i, P_{i+1} \text{ are consecutive tubelets in } V \in D_{\text{train}}\} \quad (3)$$

The temporal regularization loss penalizes first-order differences between consecutive weight spaces:

$$\mathcal{L}_{\text{temp}} = \sum_{(i, i+1) \in D_{\text{reg}}} |\theta_i - \theta_{i+1}| \quad (4)$$

where $\theta_i = g_{\phi}(\mathcal{S}_i)$ are the hyponetwork weights for clip i , and $|\theta_i - \theta_{i+1}|$ is the ℓ_1 -norm distance metric. This loss penalizes the first-order differences between weights of consecutive clips, encouraging small transitions in the weight

space. We apply this regularization to the modulated parameters θ rather than the unique parameters θ_{unq} , as we find this yields better rate-distortion performance. This parallels findings in contrastive learning, where losses applied to projected representations are often more effective than those applied to stored features (Chen et al., 2020).

4. Experimental Setup

4.1. Dataset and Training Details

We train on Kinetics-400 (Kay et al., 2017), which contains 240k training videos and 20k test videos in 400 classes, each approximately 10 seconds long. Following (Chen et al., 2024), we use a subset of 10,000 videos with 25 videos per class for training. We evaluate at three resolutions – 480p (640×480), 720p (1280×720) and 1080p (1920×1080) – and report peak signal-to-noise ratio (PSNR), structural similarity index measure (Wang et al., 2004) (SSIM) and bits-per-pixel (bpp) with encoding and decoding frames-per-second (FPS). We evaluate on UVG (Mercat et al., 2020), a Kinetics-400 validation subset, MCL-JCV (Wang et al., 2016a), and HEVC Classes B, C and E (Ohm et al., 2012; Flynn et al., 2013) which comprise videos at 1080p, 480p and 720p respectively. As memory requirements for (Chen et al., 2024) scale prohibitively with resolution, we provide comparison at 480p and 720p, and compare to NeRV (Chen et al., 2021) and HiNeRV (Kwan et al., 2023) at all resolutions. For preprocessing, videos are resized on the shorter side and center cropped. During training, a random patch-tubelet position is selected, and 8 consecutive frames are sampled per video. This contrasts with Chen et al. (2024) which encodes 8 evenly sampled frames across the video. During inference, we predict hyponetwork weights for all patch positions in each 8-frame clip, storing first predictions and residuals for subsequent clips.

4.2. Baseline Details

We compare with representative INR-based video models from two categories. Chen et al. (2024) serves as the primary hypernetwork baseline, while NeRV and HiNeRV represent per-video optimization methods, included as established baselines at higher resolutions.

NeRV-Enc* Model. We use the hypernetwork encoder from NeRV-Enc/NeRV-Dec (Chen et al., 2024) with a 5-layer HypoNeRV and adapt settings for each target resolution. Following insights from GINR (Kim et al., 2022) and NeRV-Enc, we allocate unique parameters with emphasis on the second layer. The final layer utilizes only shared base parameters without modulation. We refer to this clip-wise application of the baseline as NeRV-Enc*. Further details are provided in the Supplementary.

NeRV and HiNeRV. We use the improved NeRV architec-

ture from Chen et al. (2023) and follow the rules given for scaling. For HiNeRV (Kwan et al., 2023), we adapt the settings from the paper to the required resolution. To establish fair comparison, we configure both baselines with encoding time budgets (which include per-video training time) longer than our hypernetwork inference time and target bpp at least as high as our model.

4.3. TeCoNeRV Details

We adapt the NeRV-Enc* baseline for patch tubelets, and use a more compact 4-layer HypoNeRV while retaining the same hypernetwork encoder architecture. We calibrate the hyponetwork parameter distributions to match the pre-quantization bpp of NeRV-Enc* for fair comparison. The size of our base parameters is also much smaller than the baseline for the same train resolution (Table 2). For TeCoNeRV, we apply weight regularization finetuning after training the patch-based model (Equation (2)). For fair comparison, the baseline NeRV-Enc* and our patch-tubelet model also undergo 50 epochs of finetuning using only the reconstruction loss. Through hyperparameter search, we determine an optimal value of $\lambda_{\text{temp}} = 0.1$, and apply regularization to the modulated parameters for stable rate-distortion performance.

5. Results

Implementation Details. For NeRV-Enc*, we employ two variants of the hyponetwork, one for each of the 480p and 720p resolutions. For NeRV and HiNeRV, we train a different network for each video at each resolution and report average metrics per test dataset. For our method, we employ three configurations of non-overlapping patch tubelet models. Specifically, we use patches of size 320×160 at 480p, 320×240 at 720p and 384×270 at 1080p. We denote these models as TeCoNeRV^{1, 2, 3} in Table 1. Further details on network settings are provided in the Supplementary.

5.1. Main Results

Table 1 presents video encoding performance on UVG, HEVC, and MCL-JCV across 480p, 720p and 1080p resolutions. At 480p, TeCoNeRV achieves 25.52dB PSNR on UVG at 0.0676 bpp, a 2.47dB improvement over NeRV-Enc* (23.05dB at 0.1056 bpp) while encoding 1.65× faster, with consistent gains on HEVC and MCL-JCV. At 720p, the improvements are similarly substantial: 25.22dB versus 20.28dB on UVG, with our method encoding 3× faster. Despite their fair encoding time allocations and bitrate budgets (Section 4.2), we also outperform NeRV and HiNeRV in terms of encoding speed, quality, and bitrate.

For fair comparison, we train both NeRV-Enc* and our method on the same dataset splits – using either the 480p

Table 1. Comparison of TeCoNeRV with baselines for video encoding at resolutions 480p, 720p and 1080p. Results reported on UVG, HEVC Classes B, C and E, and MCL-JCV. Bits per pixel (bpp) is reported after quantization followed by arithmetic coding, and FPS denotes encoding / decoding speeds. Our method achieves superior PSNR and SSIM while using significantly fewer parameters. NeRV-Enc* refers to Chen et al. (2024) adapted for high-resolution videos. TeCoNeRV^{1, 2, 3} indicate configurations of our model trained with patch sizes 320×160, 320×240 and 384×270 respectively.

Method	Pretraining	Train	Test	UVG			HEVC			MCL-JCV		
				PSNR/SSIM↑	bpp↓	FPS↑	PSNR/SSIM↑	bpp↓	FPS↑	PSNR/SSIM↑	bpp↓	FPS↑
NeRV	Per Video	480p	480p	19.92 / 0.5511	0.0801	33.9 / 447.0	16.46 / 0.4424	0.0818	30.0 / 541.0	15.52 / 0.4887	0.1105	34.5 / 515.0
HiNeRV	Per Video	480p	480p	21.23 / 0.5915	0.0927	17.4 / 25.4	17.13 / 0.4607	0.0788	19.82 / 29.71	16.71 / 0.5065	0.1049	18.5 / 34.2
NeRV-Enc*	Kinetics	480p	480p	23.05 / 0.6491	0.1056	100.9 / 472.1	18.99 / 0.4694	0.1081	100.9 / 479.1	22.27 / 0.6234	0.1075	102.1 / 487.4
TeCoNeRV ¹ (Ours)	Kinetics	480p	480p	25.52 / 0.7103	0.0676	167.0 / 465.2	20.65 / 0.4970	0.0705	176.0 / 450.5	24.21 / 0.6472	0.0729	166.3 / 472.6
NeRV	Per Video	720p	720p	21.02 / 0.6402	0.0904	23.9 / 206.0	19.81 / 0.6684	0.0940	27.6 / 247.0	15.80 / 0.5187	0.1118	23.3 / 231.0
HiNeRV	Per Video	720p	720p	20.26 / 0.6437	0.0917	3.6 / 4.5	16.59 / 0.6340	0.0922	3.7 / 4.5	16.46 / 0.5427	0.1163	6.8 / 11.6
NeRV-Enc*	Kinetics	720p	720p	20.28 / 0.6426	0.1030	20.1 / 187.4	18.22 / 0.6554	0.1027	20.3 / 194.1	19.46 / 0.5941	0.1029	20.32 / 195.9
TeCoNeRV ² (Ours)	Kinetics	720p	720p	25.22 / 0.7242	0.0667	60.9 / 155.8	24.33 / 0.7430	0.0588	63.2 / 150.0	24.10 / 0.6480	0.0736	61.0 / 144.8
TeCoNeRV ² (Ours)	Kinetics	480p	720p	25.63 / 0.7380	0.0634	61.2 / 158.9	24.95 / 0.7561	0.0514	68.3 / 173.4	24.39 / 0.6578	0.0690	62.0 / 137.6
NeRV	Per Video	1080p	1080p	21.32 / 0.6739	0.0827	13.6 / 101.0	18.52 / 0.5302	0.0858	16.5 / 119.9	16.47 / 0.5450	0.1209	15.3 / 117.4
HiNeRV	Per Video	1080p	1080p	20.30 / 0.6710	0.0656	2.0 / 2.6	17.47 / 0.5267	0.0994	2.1 / 2.9	14.73 / 0.5310	0.1366	2.3 / 3.8
NeRV-Enc*	Kinetics	—	1080p	—	—	—	—	—	—	—	—	—
TeCoNeRV ³ (Ours)	Kinetics	720p	1080p	25.28 / 0.7274	0.0632	27.6 / 77.4	22.09 / 0.5682	0.0623	27.0 / 76.7	23.98 / 0.6572	0.0675	26.4 / 77.8
TeCoNeRV ³ (Ours)	Kinetics	480p	1080p	25.95 / 0.7389	0.0639	32.8 / 80.7	22.62 / 0.5794	0.0622	33.1 / 84.6	24.59 / 0.6644	0.0685	32.3 / 82.3

Table 2. Comparison of number of parameters, wall time, and memory required for training NeRV-Enc* versus TeCoNeRV. Profiled on a single NVIDIA H200 GPU with batch size 1.

Method	# Params				Wall Time † (hours)	Memory ‡ (GB)
	Train	Test	Base	Unique		
NeRV-Enc*	480p	480p	436.8K	96.3K	28	6.5
Ours	480p	480p	65.2K	15.9K	6.0 + 3.5	1.8, 2.5
Ours	720p	720p	131.0K	25.0K	6.8 + 4	2.1, 2.9
NeRV-Enc*	720p	720p	1.3M	289.0K	118	32
Ours	720p	720p	131.0K	25.0K	32 + 10	2.1, 2.9

† Total wall time: 200 epochs (NeRV-Enc*); 150+50 epochs for ours (training + finetuning).

‡ Memory: for training, then finetuning (ours only)

or 720p Kinetics video subsets. However, we also provide results with our models trained on 480p videos for inference at 720p and 1080p resolutions. This highlights a practical advantage of our patch-tubelet approach: models trained at lower resolutions can be applied to higher resolution inference, which we discuss further in Section 5.3. We observe a small boost in quality when using the 480p-trained models, which may be attributed to differences in the video subsets. Encoding and decoding speeds are measured on an NVIDIA RTX A5000 GPU for 480p and 720p resolutions, and on an RTX A6000 GPU for 1080p.

Memory and Scaling. NeRV-Enc’s computational requirements reveal a fundamental scaling limitation (Table 2). Memory grows quadratically with frame size, as the hypernetwork must predict a larger number of unique parameters, and also uses larger base parameters. With NeRV-Enc requiring 6.5GB at 480p and 33GB at 720p, training at 1080p is projected to require over 65GB (batch size 1), which makes training at this resolution slow and infeasible given our compute resources. Furthermore, the 480p→720p scaling already demonstrates poor generalization in quality, with

Table 3. Comparison of TeCoNeRV and NeRV-Enc* at 480p with ablations on residual encoding and patch-tubelets. Results reported on UVG and Kinetics-400 at 480p resolution. Our methods achieve superior quality while using significantly fewer parameters. Residual encoding (Res.) improves bpp and encoding/decoding speeds (FPS) across all models.

Method	Res.	$\mathcal{L}_{\text{temp}}$	UVG (Mercat et al., 2020)			Kinetics-400 (Kay et al., 2017)		
			PSNR / SSIM ↑	bpp ↓	FPS ↑	PSNR / SSIM ↑	bpp ↓	FPS ↑
NeRV-Enc*	✗	—	23.05 / 0.6491	0.1056	101 / 472	22.86 / 0.7208	0.1078	99 / 459
NeRV-Enc*	✓	—	23.48 / 0.6608	0.0649	284 / 544	23.17 / 0.7305	0.0698	275 / 543
Ours	✗	✗	24.92 / 0.6985	0.1045	89 / 315	24.84 / 0.7495	0.1073	89 / 313
Ours	✓	✗	25.49 / 0.7159	0.0826	125 / 337	25.28 / 0.7638	0.0861	125 / 329
TeCoNeRV	✓	✓	25.52 / 0.7103	0.0676	167 / 465	25.15 / 0.7208	0.0678	171 / 466

NeRV-Enc* achieving only 20.28dB on UVG at 720p. In contrast, our patch-tubelet decomposition maintains near-constant memory requirements regardless of resolution, enabling us to be the first hypernetwork-based approach to demonstrate results at resolutions 720p and 1080p, while previous methods report only at 256×256. While we profile on a larger H200 GPU to accommodate NeRV-Enc, our models run efficiently with batch size 32 on more accessible hardware like 4 RTXA4000 GPUs.

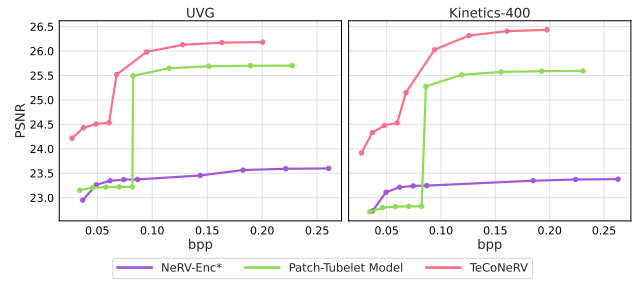


Figure 3. Quality vs. bitrate on UVG (left) and Kinetics-400 (right) at 480p. Rate-distortion curves showing PSNR vs. bpp for NeRV-Enc*, Patch-Tubelet and TeCoNeRV models. For each method, we show the Pareto frontier across two model size configurations. TeCoNeRV outperforms the baseline, achieving up to 2.47dB higher PSNR at comparable bitrates.



Figure 4. Qualitative comparison at 720p. We show 3 frames from UVG, HEVC Class E, and MCL-JCV datasets. Top to bottom: Ground truth, NeRV-Enc*, ours (“no overlap”), ours (“overlap with cropping”). Our method’s reconstructions preserve structural details, while the baseline exhibits noticeable quality degradation. Our “overlap with cropping” patch fusion strategy eliminates the boundary artifacts in ours (“no overlap”). Best viewed digitally and zoomed in.

Table 4. Rate control via patch configuration on UVG. Representative configurations with and without overlap, demonstrating quality-bitrate trade-offs at 480p, 720p, and 1080p inference.

Train	Test	Overlap	Patch Size	PSNR / SSIM ↑	bpp ↓
480p	480p	✗	320×160	25.52 / 0.7103	0.0676
480p	480p	✓	256×192	25.28 / 0.7022	0.1048
720p	720p	✗	320×240	25.22 / 0.7242	0.0667
480p	720p	✓	320×160	26.45 / 0.7533	0.0985
720p	1080p	✗	384×270	25.28 / 0.7274	0.0632
480p	1080p	✓	320×240	26.89 / 0.7572	0.0850

Impact of residual encoding. Table 3 examines our design choices in detail at 480p, evaluated on both UVG and Kinetics-400. We compare NeRV-Enc* against our patch-tubelet approach, with and without temporal coherence regularization. Residual encoding consistently improves compression efficiency across all methods while accelerating both encoding and decoding. Our Patch-Tubelet approach demonstrates significant improvements over the baseline even without temporal coherence regularization, achieving 25.49dB PSNR compared to NeRV-Enc*’s 23.48dB when both use residual encoding. Adding temporal coherence regularization yields TeCoNeRV, which maintains comparable reconstruction quality while reducing bitrate by an additional 18%, and achieving the highest encoding speed. Figure 3 illustrates the rate-distortion Pareto frontier for each method, using two size configurations across varying quantization levels (4-8 bits). TeCoNeRV consistently outperforms the baseline throughout the operating range.

5.2. Visual Quality versus Size

Our patch-based design may produce boundary artifacts, which can become more pronounced at higher resolutions. We propose to mitigate these artifacts by using strided patch-tubelets with overlap at inference. As our primary fusion strategy, we propose cropping to remove redundant edges from adjacent patches before tiling. In this way, we can

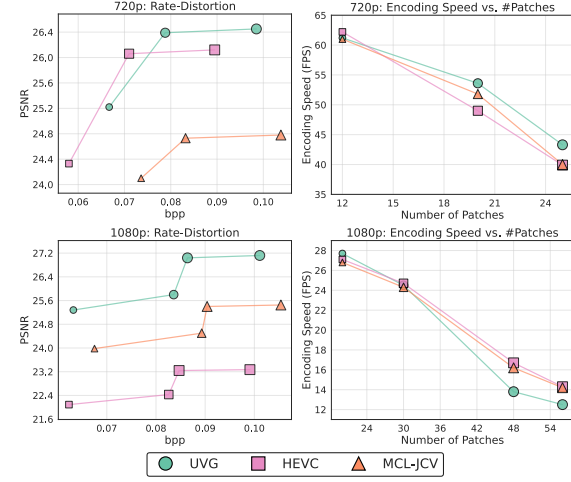


Figure 5. Rate-distortion and encoding speed vs. number of patches. Varying patch size and overlap produces different operating points at 720p (top) and 1080p (bottom) inference. Marker size corresponds to number of patches.

extend a model trained for 480p inference to infer at 720p or 1080p, even when the patch size does not exactly divide the target resolution. Figure 4 demonstrates that this approach effectively eliminates artifacts from non-overlapping patches. Additional qualitative results at 480p and 1080p are included in the Supplementary.

However, more patches may increase bitstream size, necessitating rate control. Our method provides two complementary mechanisms. First, to control patch count, we adjust patch size and overlap when scaling resolutions. For instance, while our 320×160 model trained at 480p can scale to 1080p, using the larger 320×240 model trained at 720p is more practical, producing fewer patches and a better quality-size balance. Table 4 shows representative operating points with and without overlap at each resolution. Figure 5 illustrates the full trade-off space. Second, temporal coherence strength λ_{temp} provides direct rate control

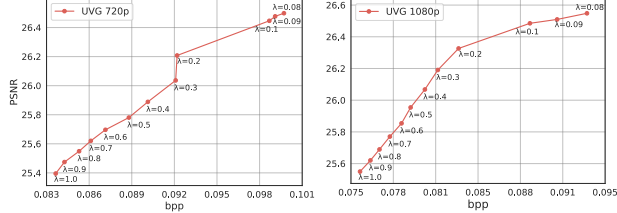


Figure 6. Rate control with temporal regularization. Finetuning our method with varying amounts of regularization (λ_{temp}) allows us to reliably trade-off PSNR and bpp, offering interpretable rate control. Left: 320×160 model (trained at 480p, inferred at 720p with overlap) on UVG, right: 320×240 model (trained at 720p, inferred at 1080p with overlap).

Table 5. Resolution-independent training on UVG. A single model trained at 480p achieves competitive quality at 480p, 720p, and 1080p. Stars (\star) and squares (\blacksquare) denote non-overlapping patches, other markers show overlap configurations.

Train	Infer	Overlap	Patch Size	PSNR / SSIM \uparrow	bpp \downarrow
★ 480p	480p	✗	320×160	25.52 / 0.7103	0.0676
★ 480p	720p	✗	320×240	25.63 / 0.7380	0.0634
★ 480p	1080p	✗	384×270	25.95 / 0.7389	0.0639
● 480p	720p	✓	320×160	26.45 / 0.7533	0.0985
● 480p	1080p	✓	320×160	27.12 / 0.7601	0.1011
● 480p	1080p	✓	320×240	26.89 / 0.7572	0.0850
■ 720p	720p	✗	320×240	25.22 / 0.7242	0.0667
■ 720p	1080p	✗	384×270	25.28 / 0.7274	0.0632
▲ 720p	1080p	✓	320×240	26.48 / 0.7479	0.0887

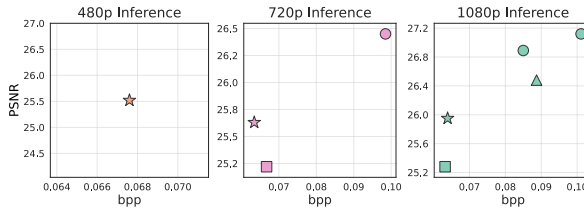


Figure 7. Our models trained at lower resolutions scale for prediction at higher resolutions. Rate-distortion curves showing competitive performance of models trained on lower-resolution videos at all target resolutions (settings in Table 5).

during finetuning. Figure 6 demonstrates that by varying λ_{temp} , we can achieve up to 18% reduction in bpp at the cost of only 4% PSNR loss, offering an interpretable mechanism for balancing quality with bitrate.

5.3. Resolution-Independent Training

Combining our patch-tubelet design with the overlap strategies in Section 5.2 enables models trained at one resolution to infer at higher resolutions. Table 1 illustrates this capability: models trained at 480p achieve competitive quality at 720p and 1080p without overlap. Similarly, models trained on 720p scale to 1080p. This allows us to train models to encode at 1080p even in the absence of high-resolution uncompressed pre-training data, which is scarce. Additionally, training a model for 720p or 1080p inference on 480p

Table 6. Impact of residual encoding at different quantization levels. We compare three encoding approaches: storing full parameters for each clip (No Residuals), residuals relative to the first clip, and residuals relative to the previous clip. Results use our TeCoNeRV model with temporal coherence regularization. At higher compression rates, residual encoding significantly outperforms direct parameter storage, with previous-clip residuals providing the best compression efficiency.

Quant Level (bits)	No Residuals		Residual from First		Residual from Previous	
	PSNR/SSIM	bpp	PSNR/SSIM	bpp	PSNR/SSIM	bpp
8	26.04 / 0.7281	0.2324	26.18 / 0.7318	0.2184	26.18 / 0.7318	0.2005
7	25.64 / 0.7174	0.1946	26.17 / 0.7313	0.1863	26.17 / 0.7314	0.1633
6	24.39 / 0.6796	0.1567	26.10 / 0.7295	0.1578	26.13 / 0.7301	0.1275
5	21.53 / 0.5774	0.1202	25.89 / 0.7228	0.1347	25.98 / 0.7253	0.0948
4	17.26 / 0.4061	0.0879	25.03 / 0.6962	0.1136	25.52 / 0.7103	0.0676

videos significantly speeds up training time. Table 5 and Figure 7 further illustrate this flexibility: a single 480p-trained model achieves strong performance across all resolutions by varying patch size and overlap at inference. Similarly, a model trained on 720p videos can infer at 1080p, and this becomes applicable to even higher resolutions, highlighting our unique paradigm. The hypernetwork learns to predict weights for fixed-size spatio-temporal regions, making resolution scaling a function of patch count rather than model capacity. This is fundamentally impossible for NeRV-Enc, which can only predict videos of a fixed resolution and whose memory constraints prevent high-resolution training.

5.4. Encoding Strategies

Table 6 compares compression efficiency across three encoding strategies: storing complete parameters for each clip, residuals relative to the first clip and residuals relative to the previous clip, across quantization levels. At aggressive quantization, direct parameter storage degrades significantly in quality, while residual encoding maintains robust performance. Thus, residual encoding not only improves compression efficiency but also enhances resilience to quantization, with previous-clip residuals providing the best quality-compression trade-off. For applications requiring random access, first-clip residuals provide direct access to any clip, or alternatively, “keyframe” clips with full parameters can be periodically inserted in the previous-clip strategy. Additional ablations on patch sizes and hypernetwork parameter distributions are provided in the Supplementary.

6. Conclusion

We address fundamental limitations of existing INR-based video compression methods. By decomposing videos into patch tubelets, we enable hypernetwork-based approaches to scale to higher resolution videos, overcoming the memory constraints that limited prior methods. We combine differential encoding with temporal coherence regularization to efficiently store only small residual weights between consecutive clips. Further, our framework enables resolution-

independent training, allowing models trained at lower resolutions to operate at higher resolutions. Notably, our method maintains fast encoding speeds of previous hypernetwork-based approaches, demonstrating that hypernetwork methods can achieve both scalability and efficiency for practical video compression. We hope this work motivates further research on improving reconstruction quality and compressed size within this representation class.

Acknowledgements. We thank Pulkit Kumar for his valuable guidance on scaling our experimental pipeline. This work was partially supported by the NSF CAREER Award (#2238769) to AS. The views and conclusions contained herein are those of the authors and should not be interpreted as necessarily representing the official policies or endorsements, either expressed or implied, of the NSF or the U.S. Government. The U.S. Government is authorized to reproduce and distribute reprints for Governmental purposes notwithstanding any copyright annotation thereon.

References

Ashkenazi, M. and Treister, E. Towards croppable implicit neural representations. *Advances in Neural Information Processing Systems*, 37:31473–31503, 2024.

Chen, H., He, B., Wang, H., Ren, Y., Lim, S. N., and Shrivastava, A. Nerv: Neural representations for videos. *Advances in Neural Information Processing Systems*, 34: 21557–21568, 2021.

Chen, H., Gwilliam, M., Lim, S.-N., and Shrivastava, A. Hnerv: A hybrid neural representation for videos. In *Proceedings of the IEEE/CVF Conference on Computer Vision and Pattern Recognition*, pp. 10270–10279, 2023.

Chen, H., Xie, S., Lim, S.-N., and Shrivastava, A. Fast encoding and decoding for implicit video representation. In *European Conference on Computer Vision*, pp. 402–418. Springer, 2024.

Chen, T., Kornblith, S., Norouzi, M., and Hinton, G. A simple framework for contrastive learning of visual representations. In *International conference on machine learning*, pp. 1597–1607. PMLR, 2020.

Chen, Y. and Wang, X. Transformers as meta-learners for implicit neural representations, 2022.

Chiang, P.-Z., Tsai, M.-S., Tseng, H.-Y., Lai, W.-S., and Chiu, W.-C. Styling 3d scene via implicit representation and hypernetwork. In *Proceedings of the IEEE/CVF winter conference on applications of computer vision*, pp. 1475–1484, 2022.

Dupont, E., Goliński, A., Alizadeh, M., Teh, Y. W., and Doucet, A. Coin: Compression with implicit neural representations. *arXiv preprint arXiv:2103.03123*, 2021.

Dupont, E., Loya, H., Alizadeh, M., Golinski, A., Teh, Y. W., and Doucet, A. Coin++: Data agnostic neural compression. *arXiv preprint arXiv:2201.12904*, 1(2):4, 2022.

Flynn, D., Sharman, K., and Rosewarne, C. Common Test Conditions and Software Reference Configurations for HEVC Range Extensions, document JCTVC-N1006. *Joint Collaborative Team Video Coding ITU-T SG*, 16, 2013.

Grill, J.-B., Strub, F., Altché, F., Tallec, C., Richemond, P., Buchatskaya, E., Doersch, C., Avila Pires, B., Guo, Z., Gheshlaghi Azar, M., et al. Bootstrap your own latent-a new approach to self-supervised learning. *Advances in neural information processing systems*, 33:21271–21284, 2020.

He, B., Yang, X., Wang, H., Wu, Z., Chen, H., Huang, S., Ren, Y., Lim, S.-N., and Shrivastava, A. Towards scalable neural representation for diverse videos. In *Proceedings of the IEEE/CVF Conference on Computer Vision and Pattern Recognition (CVPR)*, pp. 6132–6142, June 2023.

He, K., Fan, H., Wu, Y., Xie, S., and Girshick, R. Momentum contrast for unsupervised visual representation learning. In *Proceedings of the IEEE/CVF conference on computer vision and pattern recognition*, pp. 9729–9738, 2020.

Hendrycks, D. and Gimpel, K. Gaussian error linear units (gelus). *arXiv preprint arXiv:1606.08415*, 2016.

Hurri, J. and Hyvärinen, A. Simple-cell-like receptive fields maximize temporal coherence in natural video. *Neural Computation*, 15(3):663–691, 2003.

Jayaraman, D. and Grauman, K. Slow and steady feature analysis: higher order temporal coherence in video. In *Proceedings of the IEEE Conference on Computer Vision and Pattern Recognition*, pp. 3852–3861, 2016.

Jia, Z., Li, B., Li, J., Xie, W., Qi, L., Li, H., and Lu, Y. Towards practical real-time neural video compression. In *IEEE/CVF Conference on Computer Vision and Pattern Recognition, CVPR 2025, Nashville, TN, USA, June 11–25, 2024*, 2025.

Kay, W., Carreira, J., Simonyan, K., Zhang, B., Hillier, C., Vijayanarasimhan, S., Viola, F., Green, T., Back, T., Natsev, P., et al. The kinetics human action video dataset. *arXiv preprint arXiv:1705.06950*, 2017.

Khani, M., Sivaraman, V., and Alizadeh, M. Efficient video compression via content-adaptive super-resolution. In *Proceedings of the IEEE/CVF international conference on computer vision*, pp. 4521–4530, 2021.

Kim, C., Lee, D., Kim, S., Cho, M., and Han, W.-S. Generalizable implicit neural representations via instance pattern composers. *arXiv preprint arXiv:2211.13223*, 2022.

Kim, H., Bauer, M., Theis, L., Schwarz, J. R., and Dupont, E. C3: High-performance and low-complexity neural compression from a single image or video. In *Proceedings of the IEEE/CVF Conference on Computer Vision and Pattern Recognition*, pp. 9347–9358, 2024.

Kwan, H. M., Gao, G., Zhang, F., Gower, A., and Bull, D. Hinerv: Video compression with hierarchical encoding-based neural representation. *Advances in Neural Information Processing Systems*, 36:72692–72704, 2023.

Ladune, T., Philippe, P., Henry, F., Clare, G., and Leguay, T. Cool-chic: Coordinate-based low complexity hierarchical image codec. In *Proceedings of the IEEE/CVF International Conference on Computer Vision*, pp. 13515–13522, 2023.

Le Gall, D. Mpeg: A video compression standard for multimedia applications. *Communications of the ACM*, 34(4): 46–58, 1991.

Lee, H.-Y., Huang, J.-B., Singh, M., and Yang, M.-H. Unsupervised representation learning by sorting sequences. In *Proceedings of the IEEE International Conference on Computer Vision (ICCV)*, Oct 2017.

Lee, J. C., Rho, D., Ko, J. H., and Park, E. Ffnerv: Flow-guided frame-wise neural representations for videos. In *Proceedings of the 31st ACM International Conference on Multimedia*, pp. 7859–7870, 2023.

Li, J., Li, B., and Lu, Y. Deep contextual video compression. *Advances in Neural Information Processing Systems*, 34: 18114–18125, 2021.

Li, J., Li, B., and Lu, Y. Neural video compression with diverse contexts. In *Proceedings of the IEEE/CVF conference on computer vision and pattern recognition*, pp. 22616–22626, 2023.

Li, J., Li, B., and Lu, Y. Neural video compression with feature modulation. In *Proceedings of the IEEE/CVF Conference on Computer Vision and Pattern Recognition*, pp. 26099–26108, 2024.

Li, Z., Wang, M., Pi, H., Xu, K., Mei, J., and Liu, Y. E-nerv: Expedite neural video representation with disentangled spatial-temporal context. In *European Conference on Computer Vision*, pp. 267–284. Springer, 2022.

Maiya, S. R., Girish, S., Ehrlich, M., Wang, H., Lee, K. S., Poirson, P., Wu, P., Wang, C., and Shrivastava, A. Nirvana: Neural implicit representations of videos with adaptive networks and autoregressive patch-wise modeling. In *Proceedings of the IEEE/CVF Conference on Computer Vision and Pattern Recognition*, pp. 14378–14387, 2023.

Maiya, S. R., Gupta, A., Gwilliam, M., Ehrlich, M., and Shrivastava, A. Latent-inr: A flexible framework for implicit representations of videos with discriminative semantics. In *European Conference on Computer Vision*, pp. 285–302. Springer, 2024.

Mentzer, F., Agustsson, E., Tschannen, M., Timofte, R., and Van Gool, L. Practical full resolution learned lossless image compression. In *Proceedings of the IEEE Conference on Computer Vision and Pattern Recognition (CVPR)*, 2019.

Mercat, A., Viitanen, M., and Vanne, J. Uvg dataset: 50/120fps 4k sequences for video codec analysis and development. In *Proceedings of the 11th ACM Multimedia Systems Conference*, pp. 297–302, 2020.

Mildenhall, B., Srinivasan, P. P., Tancik, M., Barron, J. T., Ramamoorthi, R., and Ng, R. Nerf: Representing scenes as neural radiance fields for view synthesis, 2020.

Misra, I., Zitnick, C. L., and Hebert, M. Shuffle and learn: unsupervised learning using temporal order verification. In *Computer Vision–ECCV 2016: 14th European Conference, Amsterdam, The Netherlands, October 11–14, 2016, Proceedings, Part I 14*, pp. 527–544. Springer, 2016.

Ohm, J.-R., Sullivan, G. J., Schwarz, H., Tan, T. K., and Wiegand, T. Comparison of the coding efficiency of video coding standards—including high efficiency video coding (hevc). *IEEE Transactions on circuits and systems for video technology*, 22(12):1669–1684, 2012.

Oord, A. v. d., Li, Y., and Vinyals, O. Representation learning with contrastive predictive coding. *arXiv preprint arXiv:1807.03748*, 2018.

Padmanabhan, N., Gwilliam, M., Kumar, P., Maiya, S. R., Ehrlich, M., and Shrivastava, A. Explaining the implicit neural canvas: connecting pixels to neurons by tracing their contributions. In *Proceedings of the IEEE/CVF Conference on Computer Vision and Pattern Recognition*, pp. 10957–10967, 2024.

Rippel, O., Nair, S., Lew, C., Branson, S., Anderson, A. G., and Bourdev, L. Learned video compression. In *Proceedings of the IEEE/CVF International Conference on Computer Vision*, pp. 3454–3463, 2019.

Saragadam, V., Tan, J., Balakrishnan, G., Baraniuk, R. G., and Veeraraghavan, A. Miner: Multiscale implicit neural representation. In *European Conference on Computer Vision*, pp. 318–333. Springer, 2022.

Sen, B., Agarwal, A., Namboodiri, V. P., and Jawahar, C. Inr-v: A continuous representation space for video-based generative tasks. *arXiv preprint arXiv:2210.16579*, 2022.

Sen, B., Singh, G., Agarwal, A., Agaram, R., Krishna, M., and Sridhar, S. Hyp-nerf: Learning improved nerf priors using a hypernetwork. *Advances in Neural Information Processing Systems*, 36:51050–51064, 2023.

Sermanet, P., Lynch, C., Chebotar, Y., Hsu, J., Jang, E., Schaal, S., Levine, S., and Brain, G. Time-contrastive networks: Self-supervised learning from video. In *2018 IEEE international conference on robotics and automation (ICRA)*, pp. 1134–1141. IEEE, 2018.

Shi, W., Caballero, J., Huszár, F., Totz, J., Aitken, A. P., Bishop, R., Rueckert, D., and Wang, Z. Real-time single image and video super-resolution using an efficient sub-pixel convolutional neural network. In *Proceedings of the IEEE conference on computer vision and pattern recognition*, pp. 1874–1883, 2016.

Shin, S., Kim, S., and Oh, D. Efficient neural video representation with temporally coherent modulation. In *European Conference on Computer Vision*, pp. 179–195. Springer, 2024.

Sitzmann, V., Martel, J., Bergman, A., Lindell, D., and Wetzstein, G. Implicit neural representations with periodic activation functions. *Advances in neural information processing systems*, 33:7462–7473, 2020a.

Sitzmann, V., Zollhöfer, M., and Wetzstein, G. Scene representation networks: Continuous 3d-structure-aware neural scene representations, 2020b.

Skorokhodov, I., Ignatyev, S., and Elhoseiny, M. Adversarial generation of continuous images. In *Proceedings of the IEEE/CVF conference on computer vision and pattern recognition*, pp. 10753–10764, 2021.

Sullivan, G. J., Ohm, J.-R., Han, W.-J., and Wiegand, T. Overview of the high efficiency video coding (hevc) standard. *IEEE Transactions on Circuits and Systems for Video Technology*, 22(12):1649–1668, 2012a. doi: 10.1109/TCSVT.2012.2221191.

Sullivan, G. J., Ohm, J.-R., Han, W.-J., and Wiegand, T. Overview of the high efficiency video coding (hevc) standard. *IEEE Transactions on circuits and systems for video technology*, 22(12):1649–1668, 2012b.

Sun, C., Nagrani, A., Tian, Y., and Schmid, C. Composable augmentation encoding for video representation learning. In *Proceedings of the IEEE/CVF International Conference on Computer Vision*, pp. 8834–8844, 2021.

Tancik, M., Srinivasan, P. P., Mildenhall, B., Fridovich-Keil, S., Raghavan, N., Singhal, U., Ramamoorthi, R., Barron, J. T., and Ng, R. Fourier features let networks learn high frequency functions in low dimensional domains. *NeurIPS*, 2020.

Wang, H., Gan, W., Hu, S., Lin, J. Y., Jin, L., Song, L., Wang, P., Katsavounidis, I., Aaron, A., and Kuo, C.-C. J. Mcl-jcv: a jnd-based h. 264/avc video quality assessment dataset. In *2016 IEEE international conference on image processing (ICIP)*, pp. 1509–1513. IEEE, 2016a.

Wang, X., Farhadi, A., and Gupta, A. Actions~ transformations. In *Proceedings of the IEEE conference on Computer Vision and Pattern Recognition*, pp. 2658–2667, 2016b.

Wang, Z., Bovik, A. C., Sheikh, H. R., and Simoncelli, E. P. Image quality assessment: from error visibility to structural similarity. *IEEE transactions on image processing*, 13(4):600–612, 2004.

Wiegand, T., Sullivan, G. J., Bjontegaard, G., and Luthra, A. Overview of the h. 264/avc video coding standard. *IEEE Transactions on circuits and systems for video technology*, 13(7):560–576, 2003.

Wiskott, L. and Sejnowski, T. J. Slow feature analysis: Unsupervised learning of invariances. *Neural computation*, 14(4):715–770, 2002.

Witten, I. H., Neal, R. M., and Cleary, J. G. Arithmetic coding for data compression. *Communications of the ACM*, 30(6):520–540, 1987.

Yan, H., Ke, Z., Zhou, X., Qiu, T., Shi, X., and Jiang, D. Ds-nerv: Implicit neural video representation with decomposed static and dynamic codes. In *Proceedings of the IEEE/CVF Conference on Computer Vision and Pattern Recognition*, pp. 23019–23029, 2024.

Yu, S., Tack, J., Mo, S., Kim, H., Kim, J., Ha, J.-W., and Shin, J. Generating videos with dynamics-aware implicit generative adversarial networks. *arXiv preprint arXiv:2202.10571*, 2022.

Zhang, Y., van Rozendaal, T., Brehmer, J., Nagel, M., and Cohen, T. Implicit neural video compression, 2021.

Zhao, Q., Asif, M. S., and Ma, Z. Dnerv: Modeling inherent dynamics via difference neural representation for videos. In *Proceedings of the IEEE/CVF Conference on Computer Vision and Pattern Recognition*, pp. 2031–2040, 2023.

A. Additional Dataset Details

We primarily evaluate on the UVG (Mercat et al., 2020), HEVC (Ohm et al., 2012; Sullivan et al., 2012a) and MCL-JCV (Wang et al., 2016a) datasets. The UVG dataset consists of 7 sequences, each of 600 frames in length except for ShakeNDry, which has 300 frames. All sequences are of resolution 1920×1080 . MCL-JCV comprises 24 sequences between 120-150 frames in length, with varying amounts of motion. These sequences are provided at both 1280×720 and 1920×1080 . The HEVC standard test sequences follow the Common Test Conditions (CTC) established by ITU-T and ISO/IEC JCT-VC for benchmarking video compression algorithms. This dataset consists of five classes, A-E. We omit evaluation on classes A and D since they consist of videos significantly larger than 1080p (2560×1600) or smaller than 480p (416×240). We report on Classes B, C and E, which comprise 5 videos of size 1920×1080 , 4 videos of size 832×480 and 3 videos of size 1280×720 respectively. These videos vary between 240-600 frames in length and examples include Traffic, PeopleOnStreet, Kimono and BasketballDrive. NeRV-Enc (Chen et al., 2024) further reports on Kinetics-400. Hence, we compare against this baseline on a subset of Kinetics validation videos at 480p, consisting of one video per class. Videos are preprocessed by downsampling to the target inference resolution by resizing to 480, 720 or 1080 pixels on the shorter side with anti-aliasing and preserved aspect ratio, followed by center cropping to the exact dimensions.

B. Compression Pipeline

Our compression pipeline consists of two stages; uniform quantization followed by lossless entropy coding.

Quantization. Following prior work on video INR compression (Chen et al., 2021), we apply uniform quantization to reduce precision of model weights, significantly reducing the final model size. We quantize both the initial clip hyponetwork weights and subsequent residuals to varying bit depths (between 4-8 bits). While 8-bit quantization introduces negligible quality degradation, more aggressive quantization levels enable further compression at the cost of reconstruction quality, as demonstrated in our ablations (Table 6). We report bpp at 4 bits by default in our work, unless otherwise specified.

Entropy Coding. After quantization, we apply arithmetic coding using the torchac library (Mentzer et al., 2019) to losslessly compress the quantized weights. This produces the final bitstream, from which we compute all reported bits-per-pixel (bpp) values. Quality metrics (PSNR/SSIM) are measured after loading the compressed model and decompressing it. In Section F.5, we provide an ablation comparing arithmetic coding to Huffman coding, finding that

arithmetic coding achieves marginally better compression ratios.

Rate-Distortion Curves. To generate the rate-distortion curves in Figure 3, we train two model configurations per method – one with larger hyponetwork size and one with smaller hyponetwork size (detailed in Section D). We quantize each configuration at 4, 5, 6, 7, and 8 bits and compress with arithmetic coding. We plot quality-bitrate pairs in strictly ascending order of bitrate, forming a Pareto front, that is, if a higher-bitrate configuration achieves lower quality than a lower-bitrate one, we exclude it from the curve. This can occur, for example, when transitioning from an 8-bit quantized small model to a 4-bit quantized large model.

C. Additional Details on NeRV and HiNeRV

Frame-wise video INRs compress videos by overfitting a neural network on each video individually, predicting frames from spatial or temporal coordinates. The original NeRV (Chen et al., 2021) uses convolution-based upsampling blocks with sinusoidal positional encoding, to predict a frame at timestep t . HiNeRV (Kwan et al., 2023) introduces several improvements including grid-based positional encodings, hierarchical skip connections, patchwise processing, and bilinear upsampling with ConvNext blocks, achieving state-of-the-art reconstruction quality among frame-wise INR methods.

Note that we use the improved NeRV architecture from HiNeRV (Chen et al., 2023) and follow their scaling rules for network configuration. For HiNeRV (Kwan et al., 2023), we adapt settings from the paper to our resolutions and bitrates, tuning base size, patch size, and fc_{dim} to obtain best settings for target compression rates.

Training protocol. These per-video optimization methods typically require training for hundreds of epochs per video, with state-of-the-art models requiring hours of encoding time. Thus, for these models, encoding time includes the per-video training time. To establish fair comparison, we configure both baselines with target bpp at least as high as our model and encoding time budgets longer than our hyponetwork inference time. We train NeRV for 5 epochs per video (fewer epochs produce insufficient quality for meaningful comparison) and HiNeRV for 1 epoch per video. Quality and bpp are computed per video and averaged per dataset. While these methods can achieve better PSNR given several hours of per-video optimization, hyponetworks provide a generalizable alternative that alleviates the optimization bottleneck.

Network configurations. We use the following settings for each 600-frame UVG sequence. For NeRV, we vary $model size$, fc_{hw} , and decoder strides across resolutions:

- 480p: `modelsize` = 2.4, `strides` = [5, 2, 2, 2], f_{chw} = (12, 16)
- 720p: `modelsize` = 9.0, `strides` = [5, 2, 2, 2, 2], f_{chw} = (9, 16)
- 1080p: `modelsize` = 16.0, `strides` = [5, 3, 2, 2, 2], f_{chw} = (9, 16)

For HiNeRV, we adjust $f_{c_{dim}}$, the base grid configuration, and patch sizes :

- 480p: $f_{c_{dim}}$ = 230, `base_grid_size` = [75, 12, 16, 2], patch size = 80×80
- 720p: $f_{c_{dim}}$ = 512, `base_grid_size` = [150, 18, 32, 2], patch size = 80×80
- 1080p: $f_{c_{dim}}$ = 556, `base_grid_size` = [150, 18, 32, 2], patch size = 120×120 (This is the largest HiNeRV configuration we were able to fit on an RTX A6000 GPU at 1080p.)

Further, we scale `modelsize` (NeRV) and f_{chw} (HiNeRV) to accommodate varying video lengths in HEVC and MCL-JCV datasets. While NeRV achieves slightly faster decoding speeds than our hypernetwork approach (Table 1), it does not match TeCoNeRV’s reconstruction quality at comparable bitrates and requires substantially longer encoding times. We leave investigation of faster decoding within the hypernetwork paradigm to future work, as discussed in Section G.

D. Details of the Hypernetwork and Hyponetwork Architecture

We provide configuration details for all models evaluated in the main paper. Our architecture is based on the hypernetwork-hyponetwork framework from (Chen et al., 2024), which we briefly review before detailing configurations of the models we implement.

D.1. Framework Overview

In this architecture, a hypernetwork predicts the weights of a hyponetwork (HypoNeRV) for each input video clip. The HypoNeRV consists of multiple NeRV blocks (Chen et al., 2021), each containing convolutional layers followed by PixelShuffle (Shi et al., 2016) upsampling. This network takes a time positional encoding as input and upsamples it until it reaches the target spatial resolution. Our implementations use 4-layer (ours) or 5-layer (NeRV-Enc*) architectures with learnable convolutional parameters at each layer. Following (Chen et al., 2024), we maintain consistent convolutional channel width except for the input time position embedding (PE) and output layer (3 RGB channels).

The learnable parameters of this system are divided into base parameters and unique parameters. The base parameters encompass weights and biases across the layers of the hyponetwork, capturing common patterns and representational capacity shared across diverse video content, while unique parameters encode clip-specific information. This separation enables efficient adaptation to individual clips while maintaining a shared representational foundation.

To predict the unique parameters for a clip, the hypernetwork processes two types of tokens – data tokens representing the tokenized input clip, and a set of learnable weight tokens corresponding to layers of the hyponetwork. The Transformer backbone processes these jointly through self-attention and outputs the encoded weight tokens. These are projected via fully connected (FC) layers to convert from the transformer token dimension to the weight token dimension. The tokens are then repeated, and element-wise multiplied with base parameters, followed by normalization to yield the final modulated hyponetwork weights for the input clip (Figure 2).

In practical deployment, the hypernetwork serves as the encoder and the base parameters are installed in the decoder. Base parameters need not be transmitted per clip, they are learned once and shared across all videos. Therefore, we exclude base parameters from bitrate (bpp) calculations, considering only unique parameters and residuals.

D.2. Training Settings

All models train for 150 epochs followed by finetuning for 50 epochs (with or without temporal coherence regularization). We use the Adam optimizer with a learning rate of $1e-4$ across experiments. Input videos are organized into clips of 8 consecutive frames. This approach differs from (Chen et al., 2024), which only encodes sparsely sampled frames from videos. During training, we sample one clip per video to learn a generalizable hypernetwork. For our models, we further sample one patch-tubelet per clip. When making a prediction for the weights of the HypoNeRV, each clip is treated independently, which allows for encoding of videos of arbitrary length.

D.3. General Configuration Settings

Both NeRV-Enc* and our models use the same hypernetwork configuration, as defined in (Chen et al., 2024). Specifically, the Transformer encoder consists of 6 blocks and 12 heads, a token dimension of 720, and feedforward layers of dimension 2880, with 32×32 patch tokenization. Depending on the size of the learnable base and unique parameters, the hypernetwork size ranges from 41.1M to 47.6M parameters in our configurations. The design of the hyponetwork, including number of NeRV blocks, upsampling strides, and token distribution, varies depending

on target resolution and whether the model is patch-based (ours) or not (baseline). All HypoNeRV configurations use GELU (Hendrycks & Gimpel, 2016) activation. For fair comparison, we carefully calibrate parameter distributions for NeRV-Enc* and TeCoNeRV models at each resolution to approximately match pre-quantization bpp.

Below, we provide comprehensive configuration details for models evaluated in Tables 1-3.

D.4. NeRV-Enc* Configurations

All baseline HypoNeRV configurations use 5 NeRV blocks.

480p Resolution. For the primary NeRV-Enc* configuration evaluated at 480p in Table 1, we use the following settings:

- HypoNeRV position embedding dimension: 32, channel width (fc_{dim}): 32
- HypoNeRV kernel sizes: 1, 3, 3, 3, 3 (layers one to five)
- upscale factors (PixelShuffle strides): 5, 4, 4, 3, 2 (height) and 5, 4, 4, 4, 2 (width), for video size of 640×480
- HypoNeRV layers unique token numbers: 32, 256, 32, 24, 0; token dimensions: 200, 288, 288, 288, 0 (first layer to last)
- Hypernetwork of size 43.0M, 436.8K base parameters, 96.3K unique parameters
- Batch size: 8

For the smaller NeRV-Enc* configuration shown in Figure 3 at 480p, we use the following settings:

- HypoNeRV position embedding dimension: 20, channel width (fc_{dim}): 20
- HypoNeRV kernel sizes: 1, 3, 3, 3, 3 (layers one to five)
- upscale factors (PixelShuffle strides): 5, 4, 4, 3, 2 (height) and 5, 4, 4, 4, 2 (width).
- HypoNeRV layers token numbers: 20, 160, 20, 20, 0 token dimensions: 125, 120, 288, 180, 0
- Hypernetwork of size 42.3M, 172.0K base parameters, 31.1K unique parameters
- Batch size: 8

720p Resolution. For the NeRV-Enc* configuration tested at 720p in Table 1, we use the following settings:

- HypoNeRV position embedding dimension: 56, channel width (fc_{dim}): 56
- HypoNeRV kernel sizes: 1, 3, 3, 3, 3 (layers one to five)
- HypoNeRV upscale factors (PixelShuffle strides): 5, 4, 4, 4, 3 (height) and 5, 4, 4, 4, 4 (width), for video size of 1280×720 .
- HypoNeRV unique token numbers: 56, 448, 112, 112, 0; unique token dimensions: 350, 504, 224, 168, 0
- Hypernetwork of size 47.6M, 1.3M base parameters, 289.0K unique parameters
- Batch size: 8

As described in Section 5.1, the memory required for scaling NeRV-Enc* to 1080p is significantly larger, hence we omit this comparison and provide comparison to NeRV and HiNeRV instead at this resolution. Further, true high-resolution uncompressed video data is expensive to store and load, making such a training process difficult to execute. This highlights the advantage of our method, which allows training at lower resolutions and predicting at higher resolutions, as detailed in Section 5.3.

D.5. TeCoNeRV Model Configurations

Our patch-based models use a more compact 4-layer HypoNeRV architecture. We report three configurations corresponding to different patch sizes for inference at multiple resolutions (Table 1).

TeCoNeRV¹: 320×160 patches (480p inference). For the 320×160 TeCoNeRV¹ model evaluated at 480p inference in Table 1, we use the following settings. This is the same for the larger patch-tubelet and TeCoNeRV models in Figure 3:

- HypoNeRV position embedding dimension: 14, channel width (fc_{dim}): 14
- HypoNeRV kernel sizes: 1, 3, 3, 3 (layers one to four)
- HypoNeRV Upscale factors: 5, 4, 4, 2 (height) and 5, 4, 4, 4 (width)
- HypoNeRV unique token numbers: 5, 56, 4, 0; unique token dimensions: 196, 252, 196, 0 (first layer to last)
- Hypernetwork of size 41.3M, 65.2K base parameters, 15.9K unique parameters
- For $\mathcal{L}_{\text{temp}}$: $\lambda_{\text{temp}} = 0.1$, applied to modulated parameters θ
- Batch size: 32

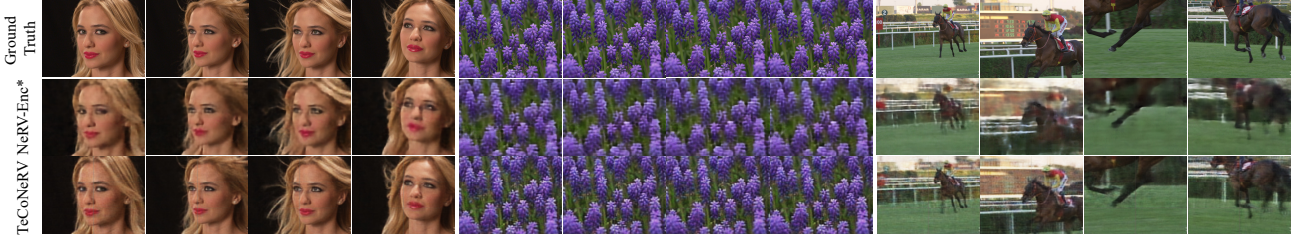


Figure 8. Visual comparison of reconstruction quality on UVG videos at 480p. The examples showcase the Beauty, Honeybee and Jockey videos from the UVG dataset, from left to right. TeCoNeRV captures finer details like facial features in Beauty, flowers in Honeybee and the horse’s legs in Jockey, which appear blurry in NeRV-Enc*. Our method preserves structural integrity and important visual elements that are sometimes missing entirely in the NeRV-Enc* reconstruction.

For the smaller Patch-Tubelet and TeCoNeRV models used in Figure 3 (Pareto front) at 480p, we keep the same settings as above and modify the HypoNeRV layers token numbers and token dimensions to be 5, 16, 4, 0 and 140, 252, 98, 0 respectively.

TeCoNeRV²: 320×240 patches (720p inference). For the 320×240 TeCoNeRV² model evaluated at 720p inference in Table 1, we use the following settings.

- HypoNeRV position embedding dimension: 16, channel width ($f_{c\text{dim}}$): 20
- HypoNeRV kernel sizes: 1, 3, 3, 3 (layers one to four)
- HypoNeRV upscale factors: 5, 4, 4, 3 (height) and 5, 4, 4, 4 (width)
- HypoNeRV unique token numbers: 10, 80, 16, 0; unique token dimensions: 200, 240, 240, 0 (first layer to last).
- Hypernetwork of size 41.5M, 131.0K base parameters, 25.0K unique parameters
- For $\mathcal{L}_{\text{temp}}$: $\lambda_{\text{temp}} = 0.1$, applied to modulated parameters θ
- Batch size: 32

TeCoNeRV³: 384×270 patches (1080p inference). For the 384×270 TeCoNeRV³ model evaluated at 1080p inference in Table 1, we use the following settings.

- HypoNeRV position embedding dimension: 20, channel width ($f_{c\text{dim}}$): 20
- HypoNeRV kernel sizes: 1, 3, 3, 3 (layers one to four)
- Upscale factors: 6, 5, 3, 3 (height) and 6, 4, 4, 4 (width)
- HypoNeRV unique token numbers: 16, 100, 16, 0; unique token dimensions: 180, 240, 180, 0 (first layer to last)

- Hypernetwork of size 41.6M, 137.5K base parameters, 29.8K unique parameters
- For $\mathcal{L}_{\text{temp}}$: $\lambda_{\text{temp}} = 0.1$, applied to modulated parameters θ
- Batch size: 32

For additional implementation details, please refer to our code.

E. Additional Results and Visualizations

E.1. Overlapping Strategies

As discussed in Section 5.2, our patch-tubelet approach enables strided inference with overlap to eliminate boundary artifacts. While we adopt cropping as our primary fusion strategy, we also evaluate blending as an alternative. Blending applies weighted averaging to overlapping regions, with position-dependent weights that fade smoothly toward patch edges. This produces slightly smoother transitions between patches compared to cropping.

Table 7 presents a detailed comparison of cropping versus blending across different overlap configurations at 720p and 1080p inference. We vary the overlap amount (in pixels, for height and width dimensions) and patch size to demonstrate the trade-off between visual quality and bitrate. Both strategies effectively remove boundary artifacts present in non-overlapping reconstructions. At 720p, blending provides marginal PSNR improvements (0.04–0.18dB) over cropping, while at 1080p, gains range from 0.13–0.18dB. Encoded bitstream size (bpp) remains identical between both strategies. However, cropping consistently achieves comparable or higher decoding FPS. We therefore adopt cropping as our default strategy for reconstruction with overlap. Encoding/decoding speeds are measured on an NVIDIA RTXA5000 for 720p inference, and RTXA6000 for 1080p inference.

Table 7. Overlapping Strategies on UVG. Varying overlap amount in pixels (height, width) and number of patches for overlap inference at 720p and 1080p. We compare cropping and blending fusion strategies in terms of reconstruction quality (PSNR/SSIM), compressed size (bpp), and encoding/decoding speeds (FPS). Both strategies effectively remove boundary artifacts, with cropping offering better speed-quality trade-offs.

Overlap (h, w)	#Patches	bpp	Cropping		Blending	
			PSNR / SSIM	FPS	PSNR / SSIM	FPS
<i>Inference at 720p (Patch Size: 320×160)</i>						
5, 0	20	0.0787	26.38 / 0.7489	51.8 / 171.4	26.42 / 0.7509	42.3 / 128.6
20, 0	20	0.0788	26.39 / 0.7500	50.4 / 170.0	26.44 / 0.7526	53.6 / 129.2
0, 5	25	0.0985	26.37 / 0.7467	42.6 / 118.4	26.54 / 0.7530	43.1 / 86.0
5, 5	25	0.0985	26.42 / 0.7508	41.1 / 140.4	26.59 / 0.7575	34.7 / 86.1
10, 10	25	0.0984	26.44 / 0.7523	35.8 / 113.8	26.61 / 0.7594	34.6 / 83.2
20, 20	25	0.0985	26.45 / 0.7533	34.1 / 114.0	26.63 / 0.7608	32.4 / 83.5
<i>Inference at 1080p (Patch Size: 320×240)</i>						
5, 0	30	0.0728	26.54 / 0.7498	26.8 / 91.6	26.57 / 0.7517	27.5 / 67.9
20, 0	30	0.0728	26.84 / 0.7542	20.8 / 74.9	26.86 / 0.7566	27.1 / 50.7
5, 5	35	0.0849	26.57 / 0.7515	22.3 / 77.0	26.69 / 0.7569	22.2 / 49.9
10, 10	35	0.0850	26.67 / 0.7537	22.4 / 74.6	26.85 / 0.7598	22.5 / 52.5
20, 20	35	0.0850	26.88 / 0.7572	22.3 / 75.8	27.01 / 0.7631	22.6 / 53.7

E.2. Additional Qualitative Results

First, we provide qualitative results comparing the reconstructions produced by TeCoNeRV with those produced by the NeRV-Enc* baseline at 480p on UVG. Figure 8 shows that while NeRV-Enc* produces reconstructions with noticeable blur and missing details, TeCoNeRV preserves structural details and object boundaries more faithfully. Further, Figure 9 shows qualitative results for TeCoNeRV at 1080p across sequences from UVG, HEVC and MCL-JCV, demonstrating that overlapping strategies – whether cropping or blending – successfully eliminate the few boundary artifacts visible in non-overlapping inference.

We provide complete video reconstructions for select sequences from HEVC and UVG at 720p and 1080p, using overlapping inference, and an HTML file for viewing these videos, with the Supplementary material. Due to the prohibitive size of uncompressed high-resolution videos of 600 frames (3.5GB+), we compress the PNG frames reconstructed by our method using the H.264 (Wiegand et al., 2003) codec with a Constant Rate Factor (CRF) of 20, to upload them as MP4 files with the Supplementary material. This secondary compression is applied solely for upload and may introduce very minor visual artifacts beyond those present in our method’s native outputs. These reconstructions are intended as research-grade demonstrations rather than production-quality outputs.

F. Ablations

F.1. Patch Tubelet Size

Table 8 examines different patch-tubelet dimensions for encoding the UVG dataset at 480p, varying both spatial partitioning strategies and parameter allocations. These ex-

Table 8. Effect of patch tubelet dimensions on reconstruction quality and compression on UVG at 480p. We evaluate different spatial partitioning strategies with varying base and unique parameter allocations. Our chosen 320×160 configuration optimally balances reconstruction quality, compression efficiency, and total patch count relative to frame resolution.

Tubelet size	PE, Ch	#Base	#Unique	PSNR / SSIM	bpp
320×160	14, 14	65.2K	15.87K	25.46 / 0.7142	0.0822
160×160	14, 14	63.7K	15.87K	26.06 / 0.7310	0.1708
160×160	14, 14	63.7K	7.94K	25.15 / 0.6981	0.0944
320×240	16, 20	130.9K	22.0K	24.17 / 0.6836	0.0737
160×160	8, 8	21.4K	10.0K	24.52 / 0.6780	0.1258
160×160	8, 8	21.4K	5.39K	24.11 / 0.6671	0.0724
160×120	8, 8	19.0K	6.56K	21.88 / 0.6132	0.1253
160×120	14, 14	56.6K	8.43K	22.21 / 0.6294	0.1517
160×80	12, 12	36.6K	6.36K	22.41 / 0.6282	0.1842
80×80	8, 8	14.4K	1.93K	21.64 / 0.6088	0.1196
80×80	4, 4	3.9K	1.54K	21.00 / 0.5724	0.0978

Table 9. Ablation on network parameter configurations for 480p encoding on UVG. We evaluate the impact of different parameter size allocations on the quality-compression tradeoff. We vary positional embedding dimensions (PE), channel widths (Ch), and the distribution of unique parameters across layers. All models use a 4-layer HypoNeRV architecture and 320×160 patches. Our selected configuration (first row) achieves strong quality-compression trade-offs with minimal base parameter overhead.

PE	Ch	Layerwise Unique Params	# Total Params		Metrics	
			Base	Unique	PSNR / SSIM	bpp
14	14	0.98K, 14.1K, 0.78K, 0	65.2K	15.87K	25.46 / 0.7142	0.0822
14	14	0.98K, 14.1K, 0.78K, 0.75K	65.2K	16.63K	24.81 / 0.6953	0.0938
14	14	0.98K, 14.1K, 0.78K, 3.02K	65.2K	18.90K	24.73 / 0.6886	0.1103
16	16	1.28K, 12.29K, 3.07K, 0	128.7K	16.64K	26.22 / 0.7353	0.0900
16	20	0.8K, 14.40K, 0.8K, 0	128.7K	16.0K	25.16 / 0.7040	0.0809
16	20	0.8K, 19.2K, 2.3K, 0	128.7K	22.3K	25.36 / 0.7067	0.1163
14	14	0.7K, 4.03K, 0.39K, 0	65.2K	5.12K	23.21 / 0.6443	0.0335
8	8	0.8K, 4.61K, 0.51K, 0	22.2K	5.92K	23.18 / 0.6482	0.0395

periments were conducted using our patch-tubelet model without temporal coherence finetuning. Smaller patches achieve higher PSNR but at increased bitrate due to the greater number of patches required. Larger patches reduce bitrate but may struggle to capture sufficient spatial detail for high-quality reconstruction, even with increased parameter counts. Our chosen 320×160 configuration optimally balances reconstruction quality, compression efficiency, and practical considerations including memory requirements and total number of patches relative to target resolution. We observe similar trends when conducting these ablations at 720p and 1080p resolutions, which we omit for brevity.

F.2. Network Parameters

Table 9 investigates how parameter allocation influences compression performance on UVG at 480p. We present variations both in base parameters (controlled by time positional embedding dimension and convolution channel width) and unique parameters (determined by token number and dimensions distributed across hyponetwork layers). For



(a) Beauty (left), Jockey (right) sequences from UVG.



(b) Kimono sequence from HEVC (left), videoSRC03 sequence from MCL-JCV (right).

Figure 9. Qualitative Results for TeCoNeRV at 1080p. Comparison of non-overlapping inference and overlapping strategies (crop and blend) for TeCoNeRV on sequences from (a) UVG and (b) HEVC, MCL-JCV. Top to bottom for each sequence: Ground truth, ours (“no overlap”), ours (“overlap with cropping”), ours (“overlap with blending”). Overlapping effectively eliminates boundary artifacts that may be visible in non-overlapping predictions, with blending producing slightly smoother transitions than cropping.

all configurations, we use 320×160 patches and a 4-layer HypoNeRV architecture with horizontal upsampling strides of 5, 4, 4, 4 and vertical upsampling strides of 5, 4, 4, 2. All experiments are conducted without temporal coherence finetuning.

Our selected configuration (first row: 65.2K base, 15.87K unique) provides a desirable quality-compression balance with minimal base parameter overhead. Increasing base parameters can improve PSNR, but with diminishing returns as parameter count grows. However, inflating base parameters while constraining unique parameters to match target bitrates is suboptimal, as larger base parameters increase memory consumption and computational overhead during both training and inference. Notably, even our most lightweight configuration (seventh row: 5.12K unique parameters) achieves 23.21dB at 0.0335 bpp, maintaining quality comparable to NeRV-Enc* while reducing bitrate by nearly 70%. These results demonstrate that strategic parameter allocation is important for efficient implicit neural video compression (Kim et al., 2022).

Table 10. Impact of clip length on reconstruction quality and compression on UVG at 480p. We vary the number of consecutive frames per clip with different parameter configurations. Our 8-frame configuration balances quality, compression efficiency, and computational overhead. PE and Ch denote position embedding dimension and convolution channel width.

#Frames	PE, Ch	#Base	#Unique	PSNR/SSIM	bpp
8	14, 14	65.2K	15.87K	25.46 / 0.7142	0.0822
4	14, 14	65.2K	15.87K	26.75 / 0.7457	0.1523
12	14, 14	65.2K	15.87K	24.18 / 0.6662	0.0606
16	14, 14	65.2K	15.87K	23.13 / 0.6517	0.0464
4	14, 14	65.2K	7.94K	25.79 / 0.7187	0.0856
4	8, 8	22.2K	5.92K	24.90 / 0.6940	0.0702
12	14, 16	83.7K	23.92K	24.22 / 0.6682	0.0909
12	16, 18	105.5K	21.24K	24.71 / 0.6877	0.0776
12	18, 18	106.3K	20.49K	24.94 / 0.6945	0.0726
16	14, 14	65.2K	32.24K	23.00 / 0.6494	0.0935
16	16, 20	128.7K	28.0K	24.95 / 0.7067	0.0757

Table 11. Ablation on distance metrics for temporal coherence regularization. We evaluate different weightings of ℓ_1 (absolute differences) and ℓ_2 (squared differences) norms in our temporal coherence loss on the 320×160 TeCoNeRV configuration for inference on UVG at 480p. Our chosen configuration ($\lambda_{\ell_1} = 0.1, \lambda_{\ell_2} = 0$) provides optimal rate-distortion performance, with higher values providing smaller size at the expense of quality. Our default configuration uses only ℓ_1 loss for the sake of simplicity, inducing sparsity in residuals.

λ_{ℓ_1}	λ_{ℓ_2}	PSNR	SSIM	bpp
0.07	0	25.62	0.7133	0.0680
0.07	0.1	25.60	0.7127	0.0683
0.08	0	25.57	0.7119	0.0681
0.08	0.1	25.56	0.7118	0.0683
0.09	0.1	25.53	0.7109	0.0680
0.1	0.0	25.52	0.7103	0.0676
0.1	0.1	25.51	0.7102	0.0676
0.12	0	25.46	0.7087	0.0662
0.2	0	25.30	0.7039	0.0631
0.2	0.2	25.29	0.7036	0.0633
0.3	0	25.13	0.6988	0.0632
1.0	0	24.53	0.6812	0.0581
2.0	0	24.07	0.6684	0.0552
3.0	0	23.72	0.6596	0.0490
5.0	0	22.96	0.6411	0.0474

F.3. Clip Length

Table 10 explores varying number of frames in a clip – 4, 12, and 16 frames compared to our main 8-frame configuration. For each clip length, we test multiple base and unique parameter configurations to ensure fair comparison across different bitrates. Shorter clips can achieve higher reconstruction quality but at increased bitrates. Longer clips reduce bitrates but may diminish quality. While the 4-frame model with reduced unique parameters (row 5: 25.79dB, 0.0856 bpp) marginally outperforms our chosen configuration, it possesses a high base-to-unique parameter ratio (65.2K vs 7.94K), also requiring twice as many predictions per video.

F.4. Temporal Coherence Loss Components

Regularization strength. As described in Section 3.4 of the main paper, our temporal coherence loss (Equation 2) is controlled by the hyperparameter λ_{temp} , which balances reconstruction quality against smoothness of weight transitions. This parameter provides a mechanism for rate control: higher values of λ_{temp} enforce stronger temporal coherence, producing smaller residuals between consecutive clips and thus lower bitrates, at the cost of some reconstruction qual-

Table 12. Impact of regularization target on compression performance. We compare applying temporal coherence regularization to unique parameters (θ_{uniq}), modulated parameters (θ), or both, across different quantization levels. We ablate on UVG both at 480p and 720p resolutions. Regularizing modulated parameters yields the best compression efficiency at lower bit depths.

Regularization Parameter Type	8 bit quant		4 bit quant	
	PSNR/SSIM	bpp	PSNR/SSIM	bpp
<i>480p</i>				
θ	26.18 / 0.7318	0.2005	25.52 / 0.7103	0.0676
θ_{uniq}	26.20 / 0.7328	0.2001	25.79 / 0.7202	0.0718
$\theta_{\text{uniq}} + \theta$	26.11 / 0.7288	0.1911	25.52 / 0.7095	0.0671
<i>720p</i>				
θ	25.68 / 0.7364	0.2035	25.22 / 0.7242	0.0667
θ_{uniq}	25.69 / 0.7400	0.2031	25.38 / 0.7324	0.0716
$\theta_{\text{uniq}} + \theta$	25.52 / 0.7335	0.1914	25.08 / 0.7220	0.0663

ity. Through hyperparameter search, we determine that $\lambda_{\text{temp}} = 0.1$ provides optimal quality-compression trade-offs for our main results. However, λ_{temp} can be adjusted based on requirements. Figure 6 demonstrates this trade-off on overlapping inference configurations. Table 11 extends this analysis with a broader range of λ_{temp} values up to 5.0 (no overlap, UVG at 480p), demonstrating the full spectrum of quality-bitrate trade-offs achievable through temporal coherence regularization.

Choice of distance metric. While our main settings for $\mathcal{L}_{\text{temp}}$ use the ℓ_1 norm for measuring weight differences (Equation 4), Table 11 also evaluates the ℓ_2 norm and their combination. The ℓ_1 norm induces sparsity by encouraging smaller weight differences to become exactly zero, resulting in more compressible residuals. The ℓ_2 norm penalizes large differences more heavily but encourages more evenly distributed magnitudes across all weights. While ℓ_2 regularization can provide marginal gains in certain configurations, ℓ_1 consistently produces more compact bitstreams. We adopt ℓ_1 as our primary distance metric for its superior compression efficiency and simplicity.

Regularization parameter mode. Table 12 investigates applying regularization to different parameter sets: pre-modulation parameters θ_{uniq} , modulated parameters θ , or both. We evaluate on UVG at both 480p resolution (320×160 patches) and 720p resolution (320×240 patches). Regularizing modulated parameters yields the best compression efficiency, particularly at lower bit depths, while regularizing both produces similar results. For simplicity, we regularize the modulated parameters in our final model.

F.5. Entropy Coding Strategies

We evaluate the impact of different entropy coding techniques on the final compression efficiency of our models.

Table 13. Entropy coding performance at varying quantization levels, on UVG at 480p. Arithmetic coding obtains marginally better bpp compared to Huffman coding across all bit depths, with the advantage increasing at lower quantization levels. Results demonstrate the complementary relationship between our temporal coherence approach and advanced entropy coding techniques.

Quant Level	PSNR/SSIM	bpp (Arithmetic)	bpp (Huffman)
8	26.18 / 0.7318	0.2005	0.2017
7	26.17 / 0.7314	0.1633	0.1646
6	26.13 / 0.7301	0.1275	0.1290
5	25.98 / 0.7253	0.0948	0.0969
4	25.52 / 0.7103	0.0676	0.0718

Table 14. Results on individual videos of the UVG dataset at 480p resolution. TeCoNeRV consistently outperforms the baseline (NeRV-Enc*) across all videos while reducing bitrates.

Video	NeRV-Enc* (Chen et al., 2024)		Ours (Patch-Tubelet)		Ours (TeCoNeRV)	
	PSNR/SSIM \uparrow	bpp \downarrow	PSNR/SSIM \uparrow	bpp \downarrow	PSNR/SSIM \uparrow	bpp \downarrow
Beauty	27.52 / 0.7822	0.1050	31.06 / 0.8268	0.0740	30.64 / 0.8138	0.0596
Bosphorus	25.59 / 0.7120	0.1030	28.26 / 0.7798	0.0734	28.14 / 0.7678	0.0620
HoneyBee	21.32 / 0.5932	0.1021	24.25 / 0.7102	0.0797	24.33 / 0.7250	0.0679
Jockey	21.78 / 0.7216	0.1106	23.68 / 0.7504	0.0949	23.91 / 0.7336	0.0739
ShakeNDry	23.81 / 0.5252	0.1025	26.43 / 0.6391	0.0791	26.22 / 0.6291	0.0680
YachtRide	23.28 / 0.6363	0.1047	25.25 / 0.6941	0.0808	25.28 / 0.6857	0.0673
ReadySteadyGo	18.43 / 0.5125	0.1096	20.00 / 0.5732	0.0947	20.46 / 0.5767	0.0746

Table 13 shows the performance of our 320×160 TeCoNeRV configuration across different quantization levels using both coding methods, on UVG at 480p. Arithmetic coding yields better compression (slightly lower bpp) than Huffman coding, with the advantage becoming more pronounced at lower bit depths, while maintaining identical reconstruction quality (as both methods are lossless transformations of the same quantized data).

F.6. Results on Individual UVG Videos

In Table 14, we present the PSNR, SSIM, and bits-per-pixel (bpp) metrics for each of the 7 videos in UVG at 480p, comparing our methods against the NeRV-Enc* baseline, at 480p. Both our patch-tubelet model and TeCoNeRV obtain better reconstruction quality-size tradeoff compared to the baseline across all sequences. TeCoNeRV further reduces bitrates (by 14-21% across videos) using temporal coherence regularization, with minimal impact on reconstruction quality.

G. Future Work

While our encoding speeds substantially improve over prior hypernetwork methods (Table 1), decoding speeds at higher resolutions (1080p) with increased number of patches can be further optimized, to match that of NeRV. Parallel decoding (forward pass through hyponetwork) across multiple GPUs where each GPU decodes of a subset of patches simultaneously, along with other optimizations, offers a promising direction to further reduce decoding latency.

Further, visual quality and bitrate still fall below established traditional and autoencoder-based codecs. However, TeCoNeRV represents an important advancement in efficiently scaling implicit neural video compression to higher resolution content. Future work could explore improved hyponetwork architectures with grid-based positional encoding. Additionally, our results are reported on an initial setup using 10,000 training videos from Kinetics. In practice, training only once on a large, diverse video corpus would yield significant further gains. Acquiring large-scale high-resolution training data and scaling the hypernetwork transformer remains an open challenge.